Investigation of the exclusive ^{3}He$(e,e'pp)n$ reaction

D. L. Groep,[1] M. F. van Batenburg,[1] Th. S. Bauer,[1,3] H. P. Blok,[1,2] D. J. Boersma,[1,3] E. Cisbani,[4] R. De Leo,[5] S. Frullani,[4] F. Garibaldi,[4] W. Glöckle,[6] J. Golak,[7] P. Heimberg,[1,2] W. H. A. Hesselink,[1,2] M. Iodice,[4] D. G. Ireland,[8] E. Jans,[1,*] H. Kamada,[6] L. Lapikás,[1] G. J. Lolos,[9] C. J. G. Onderwater,[1,2,†] R. Perrino,[10] A. Scott,[8] R. Starink,[1,2] M. F. M. Steenbakkers,[1,2] G. M. Urciuoli,[4] H. de Vries,[1] L. B. Weinstein,[11] and H. Witała[7]

[1]*NIKHEF, P.O. Box 41882, 1009 DB Amsterdam, The Netherlands*

[2]*Vrije Universiteit, de Boelelaan 1081, 1081 HV Amsterdam, The Netherlands*

[3]*Universiteit Utrecht, P.O. Box 80.000, 3508 TA Utrecht, The Netherlands*

[4]*Istituto Superiore di Sanità, Laboratorio di Fisica, INFN, Viale Regina Elena 299, Rome, Italy*

[5]*INFN Sezione di Bari, Dipartimento Interateneo di Fisica, Via Amendola 173, Bari, Italy*

[6]*Institut für Theoretische Physik II, Ruhr-Universität Bochum, D-44780 Bochum, Germany*

[7]*Institute of Physics, Jagellonian University, PL-30059 Cracow, Poland*

[8]*Department of Physics and Astronomy, University of Glasgow, Glasgow G12 8QQ, United Kingdom*

[9]*Department of Physics, University of Regina, Regina SK, Canada S4S 0A2*

[10]*INFN Sezione di Lecce, via per Arnesano, 73100 Lecce, Italy*

[11]*Physics Department, Old Dominion University, Norfolk, Virginia 23529*

(Received 9 August 2000; published 19 December 2000)

Cross sections for the ^{3}He$(e,e'pp)n$ reaction were measured over a wide range of energy and three-momentum transfer. At a momentum transfer $q=375$ MeV/c, data were taken at transferred energies ω ranging from 170 to 290 MeV. At $\omega=220$ MeV, measurements were performed at three q values (305, 375, and 445 MeV/c). The results are presented as a function of the neutron momentum in the final state, as a function of the energy and momentum transfer, and as a function of the relative momentum of the two-proton system. The data at neutron momenta below 100 MeV/c, obtained for two values of the momentum transfer at $\omega=220$ MeV, are well described by the results of continuum-Faddeev calculations. These calculations indicate that the cross section in this domain is dominated by direct two-proton emission induced by a one-body hadronic current. Cross section distributions determined as a function of the relative momentum of the two protons are fairly well reproduced by continuum-Faddeev calculations based on various realistic nucleon-nucleon potential models. At higher neutron momentum and at higher energy transfer, deviations between data and calculations are observed that may be due to contributions of isobar currents.

DOI: 10.1103/PhysRevC.63.014005 PACS number(s): 25.10.+s, 25.30.Fj, 21.45.+v, 21.30.Fe

I. INTRODUCTION

The study of exclusive two-nucleon emission by electrons at intermediate energies provides a tool to investigate the role of nucleon-nucleon correlations inside atomic nuclei. Advances in the theoretical description of light nuclei and of few-nucleon reaction processes based on modern nuclear forces allow for detailed comparisons of experimental results with calculations [1,2]. In few-nucleon systems, the Schrödinger equation, expressed in the form of Faddeev-Yakubovsky equations, can be solved exactly and the calculations can be performed based on realistic *NN* interactions such as Bonn-B, CD Bonn, Argonne v_{18}, and Nijmegen-93 I and II. The agreement between theory and data for binding energies [3] and low-energy spectra, as well as three-nucleon scattering observables, is in most cases quite remarkable.

A recent review of applications of Faddeev equations for the three-nucleon bound and scattering states occurring in processes induced by electromagnetic probes and based on realistic forces can be found in Ref. [4]. Here we report on a measurement of the ^{3}He$(e,e'pp)n$ reaction performed at the AmPS facility at NIKHEF. Data are compared to theoretical results achieved by the Bochum-Cracow Collaboration.

The cross section for electron-induced two-nucleon knockout at intermediate electron energies is driven by several processes. The *NN* interaction at small internucleon distances induces strong correlations between the nucleons inside the nucleus, which influences the momentum distributions of the bound nucleons and consequently the knock-out of nucleons by the absorption of a virtual photon via a one-body electromagnetic current. The interaction of the virtual photon with two-body currents, either via coupling to mesons or via intermediate Δ excitation, will also contribute to the cross section for one- and two-nucleon knockout. In the latter case, this contribution is expected to be largest if the virtual photon couples to a proton-neutron pair. In addition, final-state interactions (FSI) among the ejectiles influence the two-nucleon knockout cross section.

The availability of exact calculations and the well-defined final state make the trinucleon system a good candidate for two-nucleon knockout studies, since one may attempt to unravel the tightly connected ingredients of the reaction, especially short-range correlations, two-body currents, and FSI by comparison of data, measured under various kinematic conditions, with the results of these calculations.

*Electronic address: Eddy.Jans@nikhef.nl

†Present address: University of Illinois at Urbana-Champaign, 1110 West Green Street, Urbana, IL 61801-3080.

In order to investigate the reaction mechanism of two-nucleon emission and the relative importance of one-body and two-body hadronic currents in the cross section, measurements should be performed over a wide range of energy-transfer values covering the domain from the ''dip'' region to the Δ resonance. In addition, the coupling mechanism of the virtual photon to the trinucleon system may be investigated with measurements performed at various values of the three-momentum transfer. In order to extract information on the relative and center-of-mass motion of the nucleon pair, measurements covering a large angular domain and a sufficient range in kinetic energy have to be performed in a kinematic domain in which the contribution of one-body hadronic currents to the cross section dominates.

Two-proton emission from ^{3}He has been studied before by using photons produced via bremsstrahlung. The measurements were performed by Audit *et al.* [5,6] in a kinematic domain selected to emphasize the production of on-shell pions on the struck nucleon that are subsequently reabsorbed on the nucleon pair. The results were evaluated in a theoretical framework based on a diagrammatic expansion of the reaction amplitude [7]. These measurements indicated an important role for processes in which three nucleons are involved, in particular, a sequential pion exchange. Such processes were also observed at lower energy transfers, in which the initial pion is assumed to propagate off shell [8].

The use of tagged photon beams opened the possibility to perform kinematically complete measurements of the cross section for full breakup. Data obtained with the large-solid-angle detector DAPHNE [9] in the Δ resonance region, showed that the cross section for photon-induced breakup for $E_\gamma < 500$ MeV is dominated by two-step three-nucleon processes in those regions of phase space where final-state rescattering effects are minimal. No neutron momentum distribution could be extracted from this data set. The role of three-nucleon mechanisms was also observed by Kolb *et al.* [10] at lower photon energies. Neutron momentum distributions extracted from the ^{3}He$(\gamma,pp)n$ [11] and ^{3}He$(\gamma,pn)p$ [12] reactions by Emura *et al.* in the Δ-resonance region ($E_\gamma = 200$–500 MeV and 125–425 MeV, respectively) showed that both two-nucleon and three-nucleon photoabsorption mechanisms are needed to explain the data, but that at low neutron momentum the two-nucleon processes dominate the cross section. The choice of the kinematic domain and the transverse nature of the probe used in these experiments caused that the absorption of the photon by a two-proton pair was found to be largely driven by two-body hadronic currents.

The study of NN correlations by means of the $(e,e'pp)$ reaction was pioneered at NIKHEF in the ^{12}C$(e,e'pp)$ experiments by Zondervan *et al.* [13] and Kester *et al.* [14]. The advance of high duty-cycle electron accelerators has made possible the threefold coincidence experiments necessary to measure exclusive electron-induced two-nucleon knockout. Measurements performed by Onderwater *et al.* [15,16] at the Amsterdam Pulse Stretcher facility AmPS using large-solid-angle proton detectors, revealed clear signatures of short-range correlations in the ^{16}O$(e,e'pp)^{14}$C reaction. Similar results were obtained with a three-spectrometer setup at the Mainz Microtron MAMI [17]. Experimental evidence for short-range correlations was obtained by Starink *et al.* [18] from the measured energy-transfer dependence of the ^{16}O$(e,e'pp)^{14}$C$_{\text{g.s.}}$ reaction.

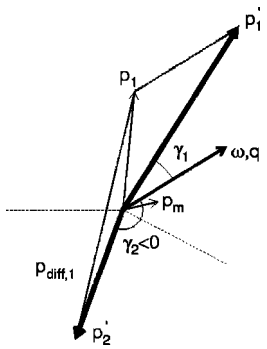

FIG. 1. Kinematic configuration of the $(e,e'pp)$ process. For clarity all momentum vectors are shown in one plane. Dotted lines represent the incoming and outgoing electron, the bold vectors the detected protons, and the thin vectors derived quantities. The reconstructed momentum vectors $\mathbf{p}_1$ and $\mathbf{p}_{\text{diff},1}$ assume coupling of the virtual photon to proton-1.

In this paper, we present results of a ^{3}He$(e,e'pp)n$ experiment performed at various values of the four-momentum transfer (ω,q) of the virtual photon. Energy and three-momentum transfer of the virtual photon were varied over a kinematic domain ranging from the ''dip'' region to just below the Δ resonance. A partial account of the present work, which is the first study of electron-induced two-proton knockout out ^{3}He, has been published in Ref. [19], where only the data taken at $\omega = 220$ MeV were discussed.

II. THEORETICAL FRAMEWORK

In the exclusive electron-induced two-nucleon knockout reaction, energy and momentum are transferred to a nucleus by a virtual photon, while after the reaction the momenta of the scattered electron and both nucleons are determined. Here we consider only those processes where the remainder of the nucleus is left intact and no secondary particles are created.

A. Kinematics and reaction mechanism

The kinematics for the ^{3}He$(e,e'pp)n$ reaction is schematically shown in Fig. 1. Within the one-photon exchange approximation the exchanged virtual photon carries an energy $\omega = E_e - E_{e'}$ and a three-momentum $\mathbf{q} = \mathbf{p}_e - \mathbf{p}_{e'}$. The two protons, with momenta $\mathbf{p}'_1$ and $\mathbf{p}'_2$, emitted after the full breakup of ^{3}He, are detected in coincidence with the scattered electron. Proton-1 is emitted at the smallest angle γ_1 with respect to $\mathbf{q}$ and is referred to as the ''forward'' proton. The second proton, emitted opposite to $\mathbf{q}$ with an angle γ_2 is referred to as the ''backward'' proton.

In an exclusive ^{3}He$(e,e'pp)n$ experiment, the final state can be reconstructed completely and the missing momentum

$$\mathbf{p}_m = \mathbf{q} - \mathbf{p}'_1 - \mathbf{p}'_2 \tag{1}$$

is equal to the momentum of the undetected neutron $\mathbf{p}'_3$. Energy conservation requires that the missing energy

$$E_m = \omega - T_1 - T_2 - T_{\rm rec} \tag{2}$$

be equal to the binding energy E_b of the ^{3}He nucleus; the excitation energy $E_x = 0$ if the reaction is confined to two-nucleon emission. Here, T_1 and T_2 are the kinetic energies of the two emitted protons, and $T_{\rm rec}$ is the kinetic energy of the recoiling neutron, which can be calculated from $\mathbf{p}_m$.

There are various ways in which the virtual photon can couple to the ^{3}He nucleus. The one-body hadronic current accounts for the absorption of a virtual photon by one nucleon of a correlated pair, which subsequently leads to the full breakup of the trinucleon system. If one assumes the coupling of the virtual photon to the proton emitted in forward direction (proton-1), one can define the momentum difference $p_{\rm diff,1} = |\mathbf{p}'_1 - \mathbf{q} - \mathbf{p}'_2|$, which in this case can be identified with $2(\mathbf{p}_1 - \mathbf{p}_2)$, where $\mathbf{p}_1$ and $\mathbf{p}_2$ are the momenta of the protons in the initial state.

Breakup of the ^{3}He nucleus can also occur via two-body hadronic currents, thus sharing the transferred momentum between two nucleons. In the energy- and momentum-transfer domain under study, two-body currents are involved in meson-exchange (MEC) and excitation of the Δ resonance followed by the decay $\Delta N \rightarrow NN$ (isobar currents or ICs). Their importance strongly depends on the isospin of the NN pair. In the case of a pp pair, the contribution of MECs to the cross section will be strongly suppressed, as the virtual photon in a nonrelativistic reduction of the current operator, does not couple to such a pair [20]. Also the contribution due to isobar currents is reduced for two protons in a relative $^1S_0$ state, as the transition via the resonant $M1$ multipole is forbidden by angular-momentum and parity-conservation rules. Therefore Δ excitation is only possible via the much weaker $C2$ and $E2$ multipoles [21]. These restrictions on MECs and ICs do not apply to pn pairs. It may therefore be expected that in a direct $(e,e'pp)$ reaction the influence of these two-body currents is reduced compared to the $(e,e'pn)$ case.

The photon can also couple to all three particles by a three-body mechanism. Sensitivity to these processes will exist at photon energies around 500–600 MeV and in specific regions of phase space, where the struck meson initially propagates on shell and is subsequently reabsorbed by the remaining nucleon pair [22].

B. Calculations

The differential cross section of the electron-induced three-body breakup of the trinucleon system has been calculated by solving consistently Faddeev-type equations for both the bound state and the final ''scattering'' state using the same nuclear forces [1,23]. Both theoretical [23,24] as well as experimental studies [25–27] indicate that rescattering among the outgoing nucleons has a significant effect on the cross sections and the spin asymmetries. The measured cross sections are compared to the results of these ''continuum Faddeev'' calculations, which completely account for these rescattering effects in the final state [28]. The calculations are based on the potential models Bonn-B, CD-Bonn, Argonne v_{18}, and Nijmegen-93, and were performed with both a non-relativistic one-nucleon current operator and with this one-body current augmented by two-body current operators.

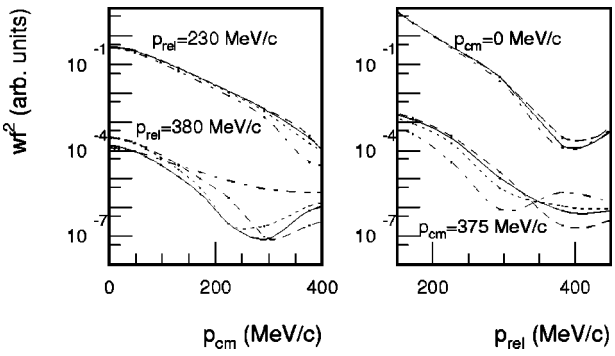

FIG. 2. Probability distribution of the ^{3}He bound-state wave function for a two-nucleon pair in a relative $^1S_0$ state, on the left-hand side displayed as a function of the center-of-mass momentum and on the right-hand side as a function of the relative momentum in the nucleon pair. The curves show calculations with the Bonn-B (solid), CD-Bonn (dashed), Nijmegen-93 (dotted), and Argonne v_{18} (dot-dashed) potential models. The domain shown is indicative for the region of phase space covered in this experiment.

From the two-body hadronic currents, only meson-exchange currents have been incorporated, using a formalism as in Ref. [29], which includes coupling to one-pion and one-ρ exchange. In order to incorporate these currents in a way compatible with the potential model used, the prescription of Ref. [30] is used. For technical details see Ref. [31].

At present, first attempts to account for Δ excitation and deexcitation within the continuum Faddeev framework are available [32], but up to now applications to electromagnetic processes have not been published. However, ample evidence exists that isobar currents are the dominant two-nucleon knockout mechanism at values of the $\gamma^* NN$ invariant mass around that of the $N\Delta$ system, and are responsible for a large part of the direct pn emission strength also at lower energy-transfer values [33]. Discussion of isobar contributions to the measured cross sections for ^{3}He$(e,e'pp)n$ is deferred to Sec. IV.

The bound-state wave function of ^{3}He has been calculated using Faddeev techniques, based on realistic models of the interaction between two nucleons [34]. In the calculations for the bound-state wave function, shown in Fig. 2, 34 channels were considered. Various types of calculations were performed, based on different models of the NN interaction. Results are shown for the Bonn-B, charge dependent (CD) Bonn, Argonne v_{18}, and Nijmegen-93 potential models. Large differences are observed between the various calculations both at high relative ($p_{\rm rel}$) and at high center-of-mass ($p_{\rm c.m.}$) momenta of the nucleons.

Direct information on the initial ^{3}He bound state can in principle be obtained from reactions induced by a one-body hadronic current; in this case, the momentum of the virtual photon is transferred to a single nucleon only. In absence of final-state rescattering, this implies that the nonstruck par-

ticles have equal momenta in the final and the initial state, and that the initial-state configuration can be reconstructed exactly from the measured proton momenta. However, the knowledge of which nucleon was hit cannot be deduced from the data, as the measured cross section [even in the plane-wave impulse approximation (PWIA)] is the coherent sum of the transition amplitudes describing coupling of the virtual photon to any of the three nucleons.

Nevertheless, insight into the coupling mechanism can been deduced from the PWIA calculations. Although the cross sections calculated with this model cannot be compared to experimental data, they are valuable to determine the relative importance of the coupling of the virtual photon to the various particles leading to the same final state. A comparison of the cross sections, calculated assuming coupling to only one nucleon, shows that, over the entire energy acceptance, the reaction is dominated by coupling to the forward proton.

III. EXPERIMENT AND ANALYSIS

The measurements were performed with the electron beam provided by the Amsterdam Pulse Stretcher facility (AmPS), with a macroscopic duty factor of 70–80 %. The incident electron energy, as determined from elastic scattering experiments, was 564 MeV and the beam current varied between 0.5 and 1.5 μA, depending on the kinematic setting. The target setup consisted of a cryogenic, high-pressure ''barrel'' cell containing gaseous ^{3}He with a nominal thickness of 268 mg cm^{-2}. A graphite target and an aluminum-oxide target were used for beam-calibration purposes and detector efficiency determination.

The scattered electrons were detected in the QDQ magnetic spectrometer. This focussing spectrometer can detect electrons within a range of $\pm 4.5\%$ with respect to the selected central momentum value. Its momentum resolution is better than 2×10^{-4} [35]. The solid angle is defined by an octangular slit with an acceptance of ± 70 mrad in both the in-plane as well as out-of-plane direction.

To detect the protons emitted from the target two scintillator detectors were used: HADRON3 and HADRON4. The design of both HADRON detectors is similar. They both cover a large solid angle (230 and 540 msr, respectively) and span a sizable range in detected proton energies. These ranges are 72 to 255 MeV for HADRON3, shielded by 5.2 mm of lead, and 47 to 180 MeV for HADRON4, shielded by 2.0 mm of stainless steel [36]. The fine-grain segmented layout, that is necessary to limit the counting rate in the individual elements to less than 1 MHz, provides an angular resolution of 0.5 (1) degrees in-plane and 1 (2) degree out-of-plane for HADRON3 (HADRON4). The proton-energy resolution amounts to 2.5% (FWHM).

In an $(e,e'pp)$ reaction, each of the three detectors (QDQ, HADRON3, and HADRON4) generates a trigger upon arrival of a particle meeting the detector-specific requirements. To determine the number of real and accidental events within the threefold coincidence time region, a *coincidence detector* is employed, which measures the arrival times of the three detector trigger signals with a resolution of 49 ps. Each trigger starts a time window with a length of 125 ns. The latter signals are used by the gating and prescaling module to classify events based on their coincidence type (single, double, or triple). The read-out of the various types of events is completely independent as long as the total event rate does not exceed 5 kHz or 1.4 MByte/s. In this experiment all threefold coincident events (triples) were stored as well as a subset of the doubles and singles for monitoring purposes.

A. Kinematic conditions

In order to enhance the contribution to the cross section due to knockout of correlated proton pairs, measurements were performed in the so-called ''dip'' region. Here, the knocked-out protons receive sufficient energy to pass the threshold for detection in both HADRON detectors, while at higher energy transfers the contribution from Δ excitation is expected to increase.

Measurements were performed at various values of the three-momentum transfer q, to investigate the coupling mechanism of the virtual photon to the ^{3}He system. The values of transferred momentum were 305 (LQ), 375 (CQW), and 445 (HQ) MeV/c, where the choice of the maximum value of 445 MeV/c was dictated by the strongly reduced count rate at higher values of q. In these measurements ω was kept constant at 220 MeV.

A series of measurements at various values of the energy transfer, ranging from 170 to 290 MeV, allowed the study of the reaction mechanism as a function of the invariant energy of the photon and two-proton final state. In this way the relative importance of one-body and two-body hadronic currents was investigated. The measurements were performed at $q=375$ MeV/c. Within the range 170–290 MeV the invariant mass of the two-proton system in the final state, $W_{p'_1p'_2}$, varies from 2005 to 2120 MeV/c^2.

The forward proton detector HADRON3 was positioned such that the angle between $\mathbf{q}$ and $\mathbf{p}_1$ was minimal, within the geometrical restrictions of detector housing and beam pipe. The positioning of the second proton detector was guided by the kinematics of quasifree two-proton emission, where at $p_m=0$ MeV/c the protons are emitted at conjugate angles.

An overview of all employed kinematic settings is listed in Table I together with the labels given for ease of reference. At the LQ kinematic setting, which features the largest flux of virtual photons, additional measurements at other proton angles were performed to investigate the angular correlation and the behavior of the cross section as a function of γ_1, the angle between $\mathbf{q}$ and the forward proton.

B. Analysis

Using established procedures, the momenta of the scattered electron [35] and of both emitted protons [36] were determined. For each of the three detectors, the trigger arrival time at the coincidence detector is measured and corrected off-line for time-of-flight differences and detector-specific delays. Based on the arrival-time differences, as

TABLE I. Overview of the kinematic configurations of the ^{3}He$(e,e'pp)$ experiment. The incident energy was 563.7 MeV.

Label	ω (MeV)	q (MeV/c)	$\theta_{e'}$ (deg.)	θ_{H3} (deg.)	θ_{H4} (deg.)
LQA	220	305	−27.72	53.8	−120.4
LQV	220	305	−27.72	53.8	−92.9
PEF	220	305	−27.72	79.9	−100.1
CQW	220	375	−40.26	53.8	−105.3
HQ	220	445	−52.01	53.8	−119.7
LW	190	375	−41.14	53.8	−119.7
IW	250	375	−38.72	53.8	−105.3
HW	275	375	−36.76	53.8	−105.3

shown in Fig. 3, various types of events can be distinguished; the peak, located at a time difference of 0 ns for both QDQ–HADRON3 and QDQ–HADRON4 coincidences, corresponds to real threefold coincidences, is superimposed on a background due to double coincident and single events. The two ridges at $\Delta t_{QH4}=0$ ns and $\Delta t_{QH3}=0$ ns are due to real $(e,e'p)$ coincidences between the scattered electron and either the backward or forward proton detector together with an accidental second proton. The ridge at $\Delta t_{QH4}=\Delta t_{QH3}$ contains real two-proton coincidences together with an accidental electron trigger. The structures sit on a flat background of events that are threefold uncorrelated.

To extract the true $(e,e'pp)$ events, the contributions of the flat background and the ridges to the region of the real coincidences have to be estimated. This is best performed by symmetrizing the coincidence time spectrum by a linear transformation

$$\tau_x=\frac{1}{\sqrt{3}}(2t_{H4}-t_Q-t_{H3}), \tag{3}$$

$$\tau_y=(t_Q-t_{H3}). \tag{4}$$

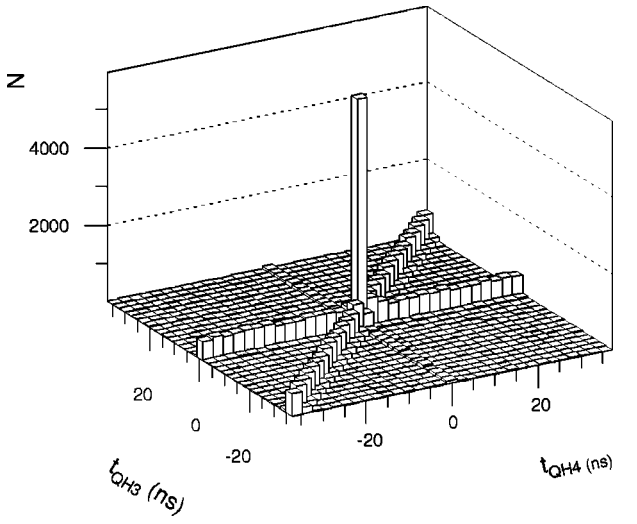

FIG. 3. Time difference distribution for three-fold coincident events, as measured in kinematics LQA ($\omega=220$ MeV, $q=305$ MeV/c).

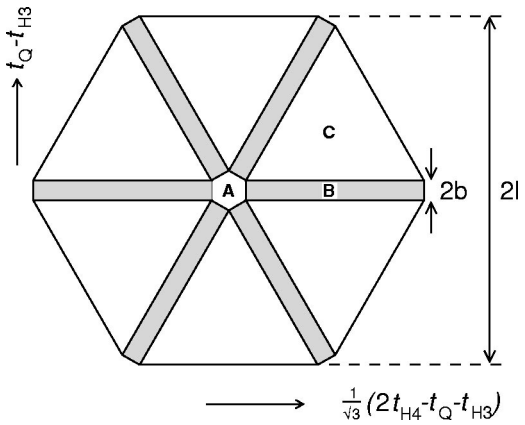

FIG. 4. A hexagonal shape is obtained in the (τ_x,τ_y) plane, after the coincidence time distributions are symmetrized.

After this transformation, the time difference distribution will exhibit a symmetric hexagonal shape as displayed in Fig. 4. The width b is chosen such that the full widths of the twofold coincidence bands are well within regions B. As the coincidence time resolution is always better than 1.5 ns (FWHM), b was chosen to be 3 ns, i.e., at least 4.5σ from the peak position.

The number of true $(e,e'pp)$ events is obtained by subtracting the number of accidental coincidences determined from regions B and C, from the number of events in the A region

$$N_T=N_A-f_BN_B-f_CN_C, \tag{5}$$

where the fractions f_B and f_C are derived from the relative lengths and surfaces of regions B and C with respect to A. Events outside regions A, B, and C are discarded. The value of l determines the accuracy with which the number of accidental coincidences in region A, where the real coincidences are located, can be estimated. This length l was chosen to be 60 ns.

The method used to subtract the accidental coincidences can be verified by inspecting the missing-energy distribution of the resulting $(e,e'pp)$ coincidences. Below the value corresponding to the two-proton separation energy, in this case the binding energy of ^{3}He, no true $(e,e'pp)$ events can occur. The missing-energy distribution of true $(e,e'pp)$ events in kinematics LQA is shown in Fig. 5. The peak corresponding to the three-body breakup of ^{3}He is located at $E_m=7.7$ MeV. The inset shows an enlargement of the E_m distribution for the range $-100<E_m<-20$ MeV. The yield in this region, -1.1 ± 1.7, is consistent with zero.

The eightfold differential cross section for the reaction ^{3}He$(e,e'pp)$ is determined as a function of various kinematic quantities such as ω or p_m. It is calculated as

$$\frac{d^8\sigma}{dV^8}(\Delta\mathbf{X})=\int_{E_x}\frac{N(\Delta\mathbf{X})}{\int\mathcal{L}dt\mathcal{V}(\Delta\mathbf{X})}\left|\frac{\partial T_2}{\partial E_x}\right|dE_x. \tag{6}$$

In this equation, $\Delta\mathbf{X}$ refers to a range of values of (a set of) kinematic quantities in which the cross section will be rep-

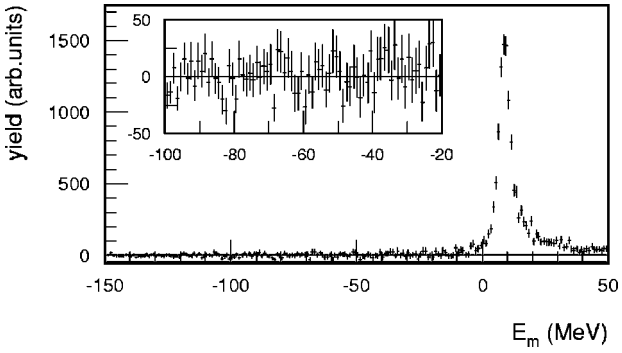

FIG. 5. Missing-energy distribution for kinematics LQA. The resolution amounts to 5.5 MeV (FWHM). The inset shows an enlargement of a subset of the same distribution.

resented, e.g., $\Delta\mathbf{X}=(\Delta p_m,\Delta p_{\mathrm{diff},1})$, $\int\mathcal{L}dt$ represents the integrated luminosity, $N(\Delta\mathbf{X})$ the number of true $(e,e'pp)$ events, and $\mathcal{V}(\Delta\mathbf{X})$ the experimental detection volume in phase space. The factor $|\partial T_2/\partial E_x|$ is a Jacobian.

The detection volume is calculated by a Monte Carlo method using 10^8 events within a nine-dimensional volume $\mathcal{V}$. It takes into account the energy and angular acceptances of the QDQ and both HADRON detectors. The sampling error due to this integration adds only 0.4% to the statistical uncertainty of the calculated cross sections.

The integration over E_x is performed in the range $-11<E_x<14$ MeV. The lower energy is set at a value corresponding to 4σ of the peak width. The events in the region at $E_x>0$ MeV correspond to true ^{3}He$(e,e'pp)$ events including events of which either the incident or the scattered electron lost energy due to the emission of a photon, resulting in a reconstructed E_x that is systematically larger than zero. The shape of this radiative tail as a function of the excitation energy was calculated using the formalism of Ref. [37]. The upper integration limit was set at $E_x=14$ MeV. For each kinematic setting, the fraction of events beyond this cutoff was calculated and applied as a correction factor to the data; this factor varies from 1.14 to 1.16. In selecting this region in excitation energy, the uncertainty due to radiative effects on the other kinematic quantities is negligible.

Because of limitations imposed by the analysis software, the integration over the E_x interval is performed on the measured yield and the detection volume separately, yielding an eightfold differential detection volume $\tilde{\mathcal{V}}$. In Fig. 6 the coverage of the $(p_m,p_{\mathrm{diff},1})$ phase space by the detection volume $\tilde{\mathcal{V}}$ is shown for the three overlapping kinematic settings at $q=305$ MeV/c.

With the experimental cross sections a systematic error of 8% is associated. This systematic error is the quadratic sum of the uncertainties in the target thickness as deduced from elastic scattering measurements (3%), the detector efficiency simulations (6%), the dead time of the electronics of the HADRON detectors (2%) and by other sources contributing less than 1% each [38].

C. Phase-space averaged theoretical cross section

The comparison of the theoretical model [28] to the data requires calculation of the cross section for specific kine-

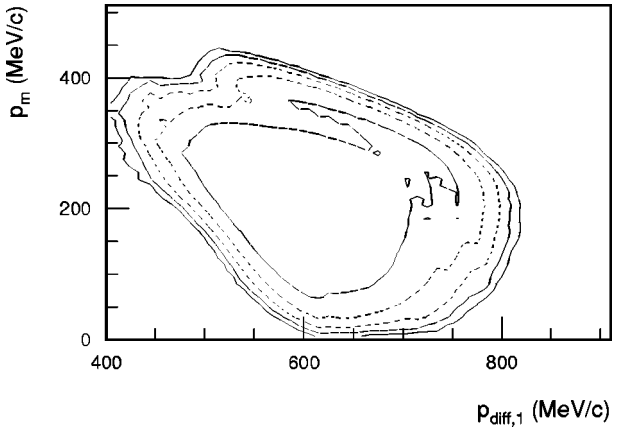

FIG. 6. Contour plot of the detection volume $\tilde{\mathcal{V}}$ as a function of $(p_m,p_{\mathrm{diff},1})$ for the combination of the kinematic settings LQA, LQV, and PEF. Contours are drawn at 30, 10, 3, 1, and 0.3 % of the maximum value.

matic configurations, as well as the evaluation and averaging of the cross section over the experimental detection volume. The theoretical cross section depends on seven kinematic variables that uniquely define the configuration. In general, the data are presented as a function of two or three quantities, derived from the basic kinematic variables. In this way an implicit averaging over the other quantities within the experimental detection volume is performed.

For a fair comparison between theory and data, the same averaging should be applied to the calculated cross sections. This averaging cannot be performed analytically because of the complexity of the integration limits, i.e., the shape of the experimental detection volume. Therefore, the integrals were approximated by a sum over an orthogonal grid. This averaging of the cross section over the experimental detection volume of each kinematics was performed for the central value of (ω,q) only, because of constraints on the available computational resources. This introduces a systematic uncertainty, which is estimated to be less than 6%, mainly due to the dependence of the cross section on the transferred three-momentum.

For a given interval in the variables in which the cross section is presented, e.g., an interval Δp_m, the average cross section is defined as

$$\left\langle\frac{d^8\sigma}{dV^8}\right\rangle\Big]_{\Delta p_m}=\frac{\int\frac{d^8\sigma}{dV^8}(\mathbf{v})D(p_m(\mathbf{v});\Delta p_m)D(\mathbf{v};\mathbf{A})d\mathbf{v}}{\int D(p_m(\mathbf{v});\Delta p_m)D(\mathbf{v};\mathbf{A})d\mathbf{v}},\quad(7)$$

where $\mathbf{v}$ is the vector representing the quantities $(\theta_1,\phi_1,\theta_2,\phi_2,T_1)$ in the laboratory system, $\mathbf{A}$ the acceptance region of the experimental detection setup, and $D(\mathbf{x};\mathbf{R})$ a two-valued function that is only different from zero if $\mathbf{x}$ is inside the region $\mathbf{R}$.

The two integrals are approximated by their sums, determined with equidistant, orthogonal grids in the laboratory quantities $\mathbf{v}$. The distance between the grid points was cho-

sen such that the resulting mean error introduced in the final result is below 6%. This corresponds to 2.5×10^6 cross-section calculations per kinematic setting for every current operator used. To verify the accuracy obtained, the cross section was calculated with a varying amount of grid points. It was concluded from these tests that a grid point density of $(\Delta\theta_1,\Delta\phi_1,\Delta\theta_2,\Delta\phi_2,\Delta T_1)=(2°,5°,4°,5°,1\ \mathrm{MeV})$ is sufficient. The error induced in the calculated cross sections is independent of the missing momentum [38].

The number of two-body angular momenta j taken into account in the NN interaction also influences the calculated cross sections. Two-body angular momenta in the NN potential up to $j=3$ have been taken into account to reach a result converged to approximately 6%.

IV. RESULTS

The cross section of the ^{3}He$(e,e'pp)$ reaction depends on seven independent kinematic variables. However, the statistical accuracy of the data does not allow representation of the measured cross section for small intervals in all seven quantities simultaneously. The character of the hadronic current operator and the ^{3}He bound-state wave function suggest that a limited set of observables carries the characteristic information of the ^{3}He$(e,e'pp)$ process.

The momentum distributions for a nucleon pair in ^{3}He shown in Fig. 2, suggest an important role for the relative momentum ($\mathbf{p}_{\mathrm{rel}}$) and the pair momentum ($\mathbf{p}_{\mathrm{c.m.}}$). Therefore, the missing momentum p_m, which in a direct $(e,e'pp)$ reaction mechanism reflects the neutron momentum in the initial state, is selected as an observable. The electron kinematics naturally define two relevant observables: the energy transfer ω and the momentum transfer q. Alternatively, at fixed q, the energy transfer ω can be replaced by the invariant energy $W_{N'N'}$ of the two nucleons of a struck pair in the final state.

Another significant process that influences the cross section is the rescattering among the outgoing nucleons. In particular, when two nucleons are emitted with (vectorially) comparable momenta the cross section will be notably enhanced. Within the experimental detection volume, such ''FSI configurations'' occur between the forward proton and the neutron. Hence, the momentum difference of these two nucleons was selected as an observable:

$$\mathbf{p}'_{ij}=\mathbf{p}'_i-\mathbf{p}'_j\,. \tag{8}$$

The ''FSI configuration'' corresponds to $p'_{ij}\rightarrow 0$ MeV/c.

Investigation of the coupling mechanisms by one-body currents shows a dominant role for coupling of the virtual photon to the forward proton. In this case, the relative momentum $\mathbf{p}_{\mathrm{rel}}$ of two nucleons in the initial state can be related to the momentum

$$\mathbf{p}_{\mathrm{diff},1}=(\mathbf{p}'_1-\mathbf{q})-\mathbf{p}'_2\overset{\triangle}{=}\mathbf{p}_1-\mathbf{p}_2\equiv 2\mathbf{p}_{\mathrm{rel}}\,. \tag{9}$$

In the following sections, the data are presented as a function of these observables and compared to the results of continuum-Faddeev calculations.

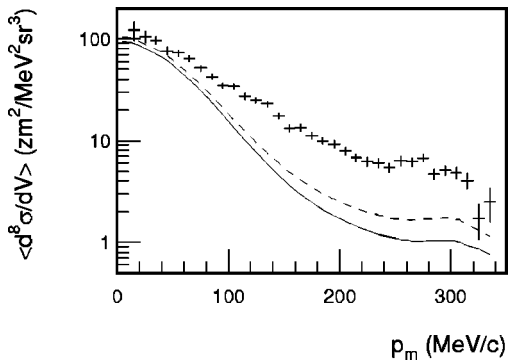

FIG. 7. Average cross section as a function of p_m for the data measured in kinematic settings LQA and LQV. The solid and dashed lines represent the results of calculations with a one-body current operator and including MECs, respectively, using the Bonn-B NN potential.

A. Neutron momentum distribution

The differential cross sections measured at the kinematics LQ are shown as a function of p_m in Fig. 7. They are averaged over the detection volume corresponding to the settings LQA and LQV, i.e., $40°<\theta_{H3}<68°$ and $-140°<\theta_{H4}<-72°$. The cross section decreases roughly exponentially as a function of the neutron momentum between zero and 300 MeV/c. This reflects the neutron momentum distribution inside ^{3}He for relative momenta in the pp pair between 250 and 330 MeV/c per nucleon, the region probed in this kinematic configuration (see Fig. 6).

Signatures of two-proton knockout by one-body hadronic currents will most likely be found at low p_m. In this domain the neutron is left with a small momentum and can be considered a spectator, since in direct pp knockout contributions from two-body currents are suppressed. As mentioned in Sec. II, contributions from MECs are prohibited in a nonrelativistic framework, as the photon will not couple to the neutral mesons exchanged in the pp pair. Additionally, the knockout via $pp\rightarrow\Delta^+p\rightarrow pp$ is suppressed since the otherwise dominant $M1$ transition is forbidden by angular momentum and parity conservation for protons initially in a $^1S_0$ state [21].

A comparison for $p_m\lesssim 100$ MeV/c with the results of continuum Faddeev calculations including only one-body currents shows a fair agreement; they account for approximately 50 to 80 % of the measured strength in this region, while the contribution of MECs is small (5%). At higher missing-momentum values, one-body calculations underestimate the data by a factor of 5. The high missing-momentum region is likely to be dominated by two-body hadronic currents (MECs and ICs), which involve coupling of the virtual photon to a proton-neutron pair. Such processes predominantly contribute to the ^{3}He$(e,e'pp)$ cross section at large p_m, because in such a process the emitted neutron has a large energy. This expectation is supported by the results of calculations with MEC contributions, which show an increased importance of MECs of up to 40% of the calculated strength at $p_m\approx 300$ MeV/c, as compared to the low p_m region. In the high p_m domain also a sizable contribution

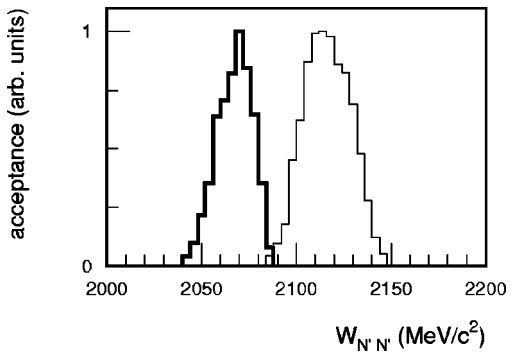

FIG. 8. Invariant mass of the two nucleons in the final state for the $p_1'p_2'$ pair at low p_m (thick line) and the $p_1'n'$ pair at high p_m (thin line) in the kinematics LQ.

from Δ-excitation can be expected: excitation of a Δ within a pn pair, a process that is not suppressed by selection rules as in the pp case, will contribute to the cross section primarily in this domain.

Excitation of the Δ resonance strongly depends on the invariant mass of the γ^*NN system. If one considers a direct reaction on a proton pair at small p_m values, the invariant mass $W_{\gamma pp}$ in the initial state can be identified with the final-state observable $W_{p_1'p_2'}$. At LQ this invariant mass ranges from 2050 to 2080 MeV/c^2, which is well below the mass of the ΔN system. If one assumes absorption of the virtual photon on a pn pair, the relevant invariant energy is that of the γ^*pn system. The corresponding invariant mass $W_{p_1'n'}$ ranges from 2100 to 2140 MeV/c^2 for p_m values around 300 MeV/c (see Fig. 8). The invariant mass of the other pn pair, i.e., $W_{p_2'n'}$, is similar to that of the pp pair for this p_m region. Therefore the cross section for intermediate Δ excitation in the p_1n pair will be dominant.

Calculations of the ^{16}O(γ,pn) cross section indicate a strong dependence of the contribution of isobar currents on the photon energy [33]. These calculations, as well as calculations of photon-induced deuteron breakup, which use a different Δ propagator [39], indicate a maximum in the cross section due to Δ excitation around $E_\gamma \approx 250$ MeV. This corresponds to an invariant mass $W_{p_1'n'}$ around 2125 MeV/c^2, which is at the center of our acceptance for the LQ kinematic setting.

The excitation of the Δ resonance and the subsequent decay of the ΔN system in a pn pair is expected to cause—due to its multipole character—a characteristic angular dependence of the cross section. This can also be seen in calculations of the $^{16}O(\gamma,pn)$ cross section at $E_\gamma = 281$ MeV, a reaction that is also dominated by the isobar current [40]. In this reaction the cross section reaches a maximum between approximately $\gamma_1 = 40°$ and 100°, depending on the proton energy T_1. In Fig. 9 the angular dependence of the measured ^{3}He$(e,e'pp)$ cross sections is shown for the missing momentum interval from 230 to 250 MeV/c. The data exhibit a characteristic angular dependence: at larger angles γ_1 a strong increase is observed that is not reproduced by the calculation based on a one-body current operator or those including MECs.

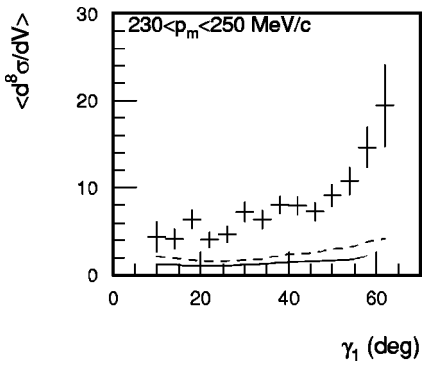

FIG. 9. Average cross section as a function of γ_1 for the p_m interval from 230 to 250 MeV/c for the combined kinematic settings at $q = 305$ MeV/c. Curves as in Fig. 7.

B. Momentum-transfer dependence

Further information on the reaction mechanism is obtained from the dependence of the cross section on q. The data at the various (ω,q) points all show a similar dependence of the cross section on the missing momentum. This is expected for quasifree two-proton knockout, in which the neutron acts as a spectator, implying that the effects due to final-state interactions are generally small. However, strong rescattering effects may occur at specific values of p_m, because $p_{13}' \rightarrow 0$ MeV/c, the exact position of which depends on the experimental detection volume. Therefore, no reliable comparison can be made between data of different (ω,q) settings for kinematic domains in which an ''FSI configuration'' occurs. For the q-scan data, the rescattering effects limit the usable domain to $p_m \lesssim 220$ MeV/c.

In Fig. 10 the cross section is shown as a function of q for two slices in p_m. The data at missing-momentum values below 100 MeV/c show a decrease by a factor of 4 between $q = 305$ MeV/c and $q = 375$ MeV/c. Both this slope and the absolute magnitude of the cross sections are reasonably well described by the calculations. For both values of the momentum transfer a calculation with only one-body hadronic cur-

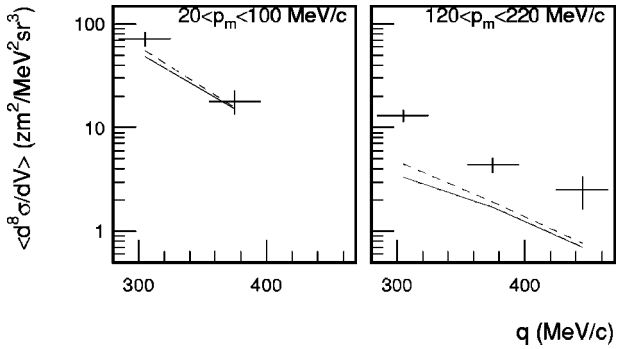

FIG. 10. Average cross-section dependence on the momentum transfer q, for two slices in the final-state neutron momentum at $\omega = 220$ MeV. Curves are the same as in Fig. 7. The data were averaged over the domain $10° < \gamma_1 < 25°$. The horizontal error bars indicate the range in q values covered due to the acceptance of the spectrometer. The domain $p_m < 120$ MeV/c is not covered by the detection volume of the HQ kinematic setting.

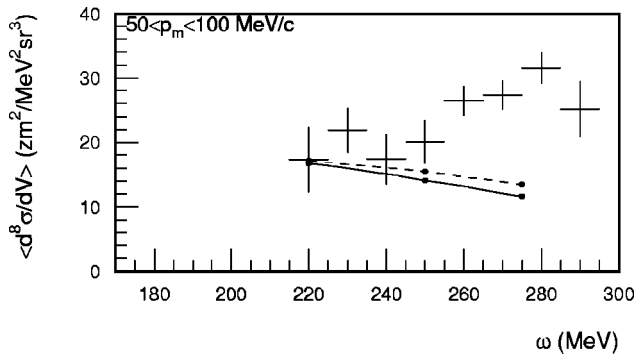

FIG. 11. Average cross section as a function of the energy transfer ω at $q=375$ MeV/c and $50<p_m<100$ MeV/c. Curves as in Fig. 7.

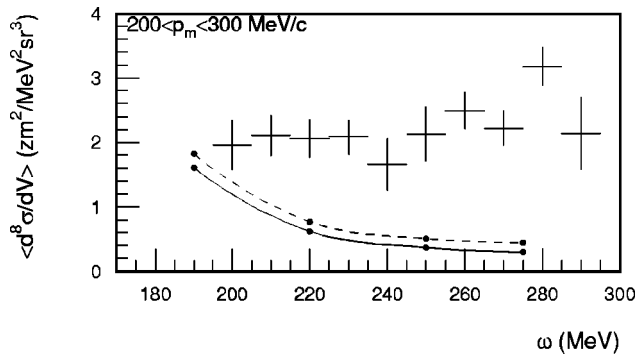

FIG. 12. Average cross section as a function of the energy transfer ω at $q=375$ MeV/c and $200<p_m<300$ MeV/c. Curves as in Fig. 7.

rents accounts for $72\pm13\%$ of the measured strength. The inclusion of MEC contributions has—as expected—only a minor effect and increases the calculated strength to 80% of the experimentally observed value. The fair agreement between data and theory for both momentum transfer values indicates that, in the p_m domain below 100 MeV/c, the cross section is predominantly driven by a one-body reaction mechanism.

In the p_m domain $120<p_m<220$ MeV/c, the difference between a one-body calculation and data is about a factor of 5. Inclusion of MECs in the calculation increases the calculated cross section by 10 to 35 %, depending on the momentum transfer, thus reducing the discrepancy to about a factor of four. The q-dependence of the data and the calculations is nevertheless similar.

C. Energy-transfer dependence

As discussed in the previous section, the low p_m region is most likely due to direct two-proton knockout, as in this domain the neutron is left ''at rest.'' In case of such a direct reaction mechanism, the invariant mass of the two emitted protons $W_{p_1'p_2'}$ can be identified with the invariant mass of the γpp system. For $p_m<100$ MeV/c, this invariant mass ranges from 2055 MeV/c^2 at $\omega=220$ MeV (well below the Δ resonance) to 2120 MeV/c^2 at $\omega=290$ MeV, i.e., almost on top of the resonance.

In Fig. 11 the data for the p_m domain from 50 to 100 MeV/c at $q=375$ MeV/c are displayed as a function of the energy transfer ω. The calculations performed with a one-body current operator show a slightly decreasing trend as a function of ω, which is due to changes in the relative momentum of the pp pair in the initial state probed in the reaction; whereas at $\omega=220$ MeV the central value for the relative momentum is 290 MeV/c per nucleon, it has risen to 360 MeV/c per nucleon at $\omega=275$ MeV.

As expected from the data shown in Sec. IV B, the agreement between data and calculations for $\omega\approx220$ MeV is quite good, which can be considered as evidence for the dominance of one-body currents in this p_m and ω domain. The inclusion of MECs in the calculation hardly changes the cross section at $\omega=220$ MeV.

At energy transfer values in the range from 220 to 290 MeV, the data show an increase of almost 50%. The contribution due to MECs remains rather low (below 15%). Therefore, the increase of the experimental cross section probably reflects an increasing importance of intermediate Δ excitation at higher invariant masses $W_{p_1'p_2'}$.

Similarly, the cross section as a function of ω for the missing momentum region from 200 to 300 MeV/c is shown in Fig. 12. The cross sections calculated with a one-body current operator decrease systematically for increasing values of ω, again due to the increasing relative momentum of the protons in the pp pair. In addition, at $\omega\approx200$ MeV, the kinematic variables are close to an ''FSI configuration'' occuring within the experimental detection volume at $p_m=320$ MeV/c. The measured cross section does not show pronounced dependence on ω. At the lowest ω value, the ratio of the experimental and theoretical cross section is 1.6 ± 0.3, whereas at higher values of the energy transfer the data overshoot the theoretical results by about a factor of 5.

In the p_m domain probed here, a considerable part of the strength may be due to coupling of the virtual photon to a pn pair, whose invariant mass in the final state is considerably larger than in the γpp system: $2110<W_{p_1'n'}<2190$ MeV/c^2 for $250<p_m<300$ MeV/c. This domain corresponds to the region where the total cross section for photon-induced deuteron breakup reaches its maximum, i.e., at $E_\gamma\approx265$ MeV [21]. This corresponds to an invariant mass of the γpn system of approximately 2140 MeV/c^2. In this energy range, the photoinduced breakup of the deuteron is known to be dominated by intermediate Δ excitation and its subsequent decay.

D. Rescattering configurations

For kinematic domains in which two nucleons are emitted with similar momentum vectors, rescattering effects can influence the cross section considerably. The presentation of the data as a function of the momentum difference p_{ij}' allows an investigation of these rescattering effects.

In the HQ kinematic setting the detection volume extends to $p_{13}'=0$ MeV/c. A good agreement between the data obtained at $\omega=220$ MeV at p_m values below 100 MeV/c and continuum-Faddeev calculations based on a one-body had-

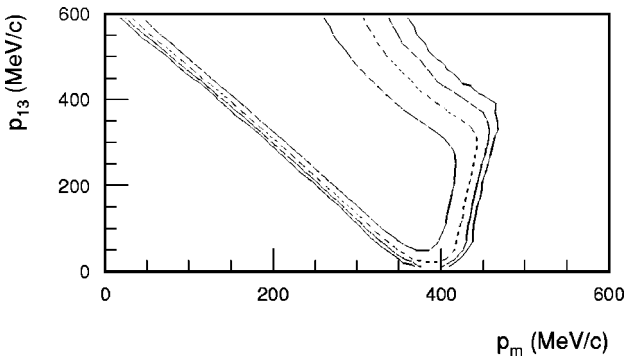

FIG. 13. Projection of the detection volume on the (p'_{13},p_m) plane for kinematics HW.

ronic current was shown already in Ref. [19]. Similar configurations occur at other kinematic settings. As the cross section depends strongly on both p'_{13} and p_m individually and the detection volume is nonrectangular in these two observables (see Fig. 13), one can reduce these rescattering effects by limiting the p_m range.

In particular the HW kinematics contains a fairly broad region in p_m—between 360 and 410 MeV/c—for which the region around $p'_{13}=0$ MeV/c is covered by the detection volume (see Fig. 13). Unfortunately, the high value of energy transfer together with the high p_m region means that a sizable part of the reaction occurs via intermediate Δ excitation in the pn pair. This has the consequence that the calculated cross section, even including MECs, globally underestimates the data by a factor of 4.4 at $360<p_m<410$ MeV/c (and by a factor of 9.1 with respect to a one-body calculation) as can be seen from Fig. 14.

Although the absolute magnitude is not correctly predicted, the dependence of the cross section on p'_{13} is well reproduced by both the one-body calculations and those including MECs. The similarity in shape between both types of calculations suggests that the dependence of the cross section

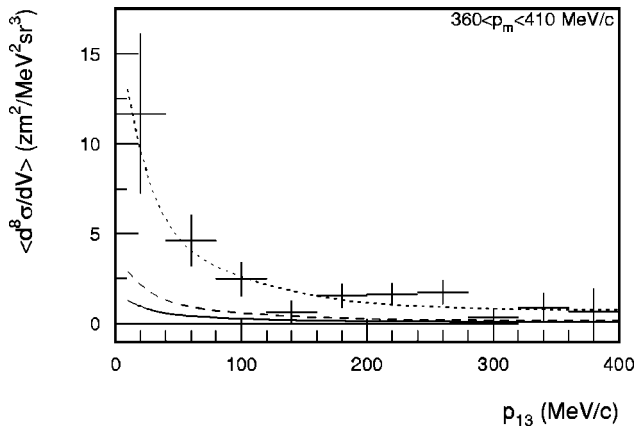

FIG. 14. Average cross section for the ''FSI configuration'' at kinematics HW. The p_m acceptance has been limited to $360<p_m<410$ MeV/c. The curves are results of the Faddeev calculations with a one-body current operator (solid), including MECs (dashed) and a scaled ($\times 4.43$) MEC result (dotted), all based on the Bonn-B potential.

on p'_{13} is mainly due to NN rescattering and the magnitude to the current operators used. Scaling of the calculated cross sections that include MECs, by a factor of 4.43 results in a good agreement between data and calculations over the entire p'_{13} domain. Hence, although the calculations do not adequately describe the absorption of the virtual photon by the nucleon pairs, it is likely that the continuum Faddeev calculations adequately describe final-state rescattering effects.

E. Relative momenta and potential models

An investigation of the data at low missing momentum, i.e., $p_m \lesssim 100$ MeV/c, and at an energy transfer value of $\omega = 220$ MeV, showed a dominant contribution from direct two-proton knockout by a one-body hadronic current. As argued, breakup induced by coupling to a one-body current in principle allows investigation of the ^{3}He bound-state wave function. The calculations indicate that the cross section in this domain is almost exclusively determined by coupling of the virtual photon to the forward proton. Hence, according to the calculations, the observable $p_{\mathrm{diff},1}$ as defined in Eq. (9) should be representative of the initial-state proton momentum p_1. Investigation of the cross section as a function of $p_{\mathrm{diff},1}$ in the low p_m domain at LQ may thus lead to insight in the initial-state wave function of ^{3}He.

In Fig. 2, the probabilities associated with the ^{3}He wave function are shown as a function of the relative momentum of a nucleon pair for various NN potentials. The shape of the wave functions within the experimentally accessible domain is similar for Bonn-B, CD-Bonn, and Nijmegen-93. The result for the Argonne v_{18} potential is different, especially in the high p_{cm} and high p_{rel} region, but as in this domain two-body currents are expected to give a significant contribution to the $^3\mathrm{He}(e,e'pp)$ cross section, no quantitative comparison to the data can be made. However, small differences in magnitude exist among the various model predictions for low p_m, and also here the difference is largest for Argonne v_{18}. One expects for all potential models a decrease of the experimental cross section due to one-body currents as a function of $p_{\mathrm{diff},1}$, because the probability density decreases as a function of p_{rel}. At higher missing momenta, the cross section dependence becomes increasingly more flat.

The rapid changes in cross section as a function of p_m make it necessary to investigate the dependence on $p_{\mathrm{diff},1}$ for slices in the missing momentum, that are not wider than 20 MeV/c. The data in the two graphs of Fig. 15 are taken from adjacent slices in p_m (from 50–70 and from 70–90 MeV/c). These already show a different dependence on p_{diff}. The fine binning thus required leads to a reduced statistical accuracy for the measured cross sections.

It was already shown in Fig. 7 and Fig. 10 that in the domain $p_m \lesssim 100$ MeV/c the dependence of the cross section on p_m and q is fairly well reproduced by calculations performed with the Bonn-B potential. Figure 15 shows that also the dependence of the cross section on the momentum difference $p_{\mathrm{diff},1}$ [see Eq. (9)] in this p_m domain is quite well reproduced by the calculations.

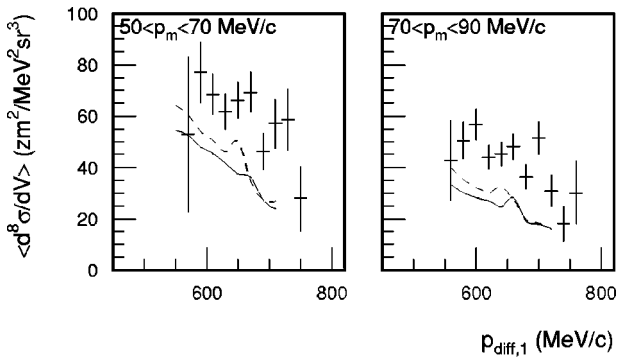

FIG. 15. Average cross section as a function of $p_{\mathrm{diff},1}$ for two slices in p_m of 20 MeV/c wide. Data are taken from the combined kinematic settings LQA, LQV, and PEF. Solid curves are based on one-body currents only; dashed curves include MECs, both calculated using the Bonn-B potential. The wiggles in the calculated cross section are due to small variations in the parts of the detection volume that contribute in the different kinematic configurations.

In Fig. 16 the same data are compared to predictions from continuum Faddeev calculations, performed with different NN-potential models. Differences in both magnitude and slope are observed, with the Argonne v_{18} prediction being up to 15% lower than the one based on Bonn-B.

The variations between the calculations performed with the various models are of the same order of magnitude as the effects of MECs, which was only calculated using the Bonn-B potential. The influence of intermediate Δ excitation on the calculated slope is as of yet unknown; also the underestimation of the data by all four calculations, which amounts to approximately 30% at $50<p_m<90$ MeV/c, is still not explained quantitatively. In the missing-momentum region above 200 MeV/c, the differences in the calculated cross section due to the NN potential are almost negligible within the experimentally probed domain. In view of these uncertainties, the low p_m data do not yet suggest a preference for any of the potential models.

V. SUMMARY AND CONCLUSIONS

In summary, the cross sections for the exclusive reaction ^{3}He$(e,e'pp)n$ were measured for three values of the three-momentum transfer of the virtual photon ($q=305$, 375, and 445 MeV/c) at an energy transfer value ω of 220 MeV. At $q=375$ MeV/c, measurements were performed over a continuous range of transferred energy from 170 to 290 MeV. At $q=305$ MeV/c, a large range in center-of-mass ($p_{\mathrm{c.m.}}=0$ to 310 MeV/c) and pp relative ($p_{\mathrm{diff},1}=500$ to 800 MeV/c) momenta was covered. The data are compared to results of continuum Faddeev calculations that account for the contributions of rescattering among the emitted nucleons. These calculations include both one-body hadronic currents as well as contributions due to the coupling of virtual photon to π and ρ mesons exchanged between two nucleons in an intermediate state (meson-exchange currents or MECs). Various potential models were used in the calculations: Bonn-B, charge-dependent (CD) Bonn, Nijmegen-93, and Argonne v_{18}.

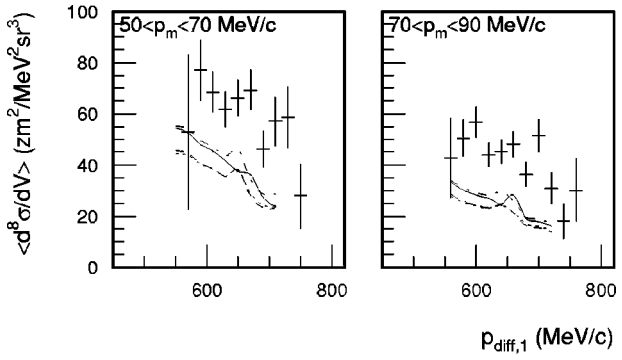

FIG. 16. Average cross section as a function of $p_{\mathrm{diff},1}$ as in Fig. 15. All curves are based on one-body currents only, but calculated using various models for the NN potential: solid curves Bonn-B, dashed curves CD-Bonn, dotted curves Argonne v_{18}, dot-dashed curves Nijmegen-93.

Calculations performed with only a one-body hadronic current operator show a fair agreement with the data obtained at $p_m \lesssim 100$ MeV/c at $\omega=220$ MeV and $q=305$ MeV/c. Measurements performed at $q=375$ MeV/c show similar results. Here, the inclusion of MECs in the current operator only has a minor effect on the calculated strength. It can therefore be concluded that at $\omega=220$ MeV and $p_m<100$ MeV/c the cross section is dominated by direct knockout of two protons via a one-body hadronic current. At higher p_m values, from 120 to 320 MeV/c, a discrepancy of up to a factor of 5 is observed between the data and calculations with a one-body current operator only. Contributions due to MECs increase the calculated strength by up to 35% at most.

The influence of intermediate Δ excitation depends on the invariant mass of the γ^*NN system involved. To investigate such isobar currents, measurements were performed in the domain $\omega=170$–290 MeV. This range corresponds for $p_m<100$ MeV/c to invariant masses $W_{p'_1p'_2}$ between 2055 and 2120 MeV/c^2. An increase of the measured cross section by almost 50% is seen over this range in energy transfer. Theoretical predictions including MECs underestimate the data from 30% at $\omega=220$ MeV to a factor of 2 at the higher ω values, presumably reflecting the increased importance of the Δ resonance.

At higher neutron momentum values, data and theoretical predictions differ up to a factor of 5 for all values of ω. This is likely due to intermediate Δ excitation by the virtual photon of the pn pair, for which the invariant mass in the final state amounts to approximately 2150 MeV/c^2. This value corresponds to the position of the resonance in deuteron electrodisintegration. A further indication for the importance of intermediate Δ excitation as a process contributing to the ^{3}He$(e,e'pp)$ cross section in the p_m domain above 100 MeV/c can be found in the dependence of the cross section on the forward proton emission angle γ_1. Comprehensive treatment of the Δ degrees-of-freedom within the continuum Faddeev framework is necessary before quantitative conclusions can be drawn from the data measured at high p_m or high ω values.

Within the experimental detection volumes covered in the measurement at $(\omega,q)=(220\ \mathrm{MeV},445\ \mathrm{MeV}/c)$ and

(275 MeV,375 MeV/c) and a selected domain in p_m, two nucleons are emitted with a low relative momentum in the final state. In these regions, rescattering effects strongly influence the cross section. Data from such specific ''FSI configurations'' provide a good tool to check the calculations in this respect. Good agreement was found between data measured at $\omega=220$ MeV and $q=445$ MeV/c, and theoretical predictions, when presented as a function of the pn momentum difference in the final state. Data obtained at $\omega=275$ MeV and $q=375$ MeV/c confirmed this result, although the absolute magnitude of the cross section is underestimated by the predictions, probably due to lack of isobar contributions in the current operator used.

Information on the relative momentum of the two protons in ^{3}He may be obtained in the domain $\omega\approx220$ MeV and $p_m<100$ MeV/c, since in this domain knockout is expected to be dominated by direct pp emission via a one-body hadronic current. The observed decrease of the cross section as a function of relative momentum reflects the behavior of the wave function and is well reproduced by calculations at low p_m. Calculations performed with different models of the NN interaction lead to different predictions of the cross section in this domain, both in magnitude and as a function of $p_{\rm rel}$. The statistical and systematic uncertainties of the data, as well as the sizeable changes induced in the predictions by the MECs and the unknown influence of isobar contributions, do not yet permit us to express preference for any of the potential models considered.

Larger differences between the wave functions calculated from the various NN potentials are observed at high center-of-mass momentum values and for relative momenta above 400 MeV/c per nucleon. However, the interpretation of this domain awaits either a better theoretical treatment of the high p_m region or experimental means to isolate the contribution of isobar currents to the cross section. In this respect, separation of the ^{3}He$(e,e'pp)$ cross section in its contributing structure functions and an investigation of the complementary reaction ^{3}He$(e,e'pn)$ will provide valuable information for better understanding the processes involved.

ACKNOWLEDGMENTS

This work is part of the research program of the Foundation for Fundamental Research on Matter (FOM) and was sponsored by the Stichting Nationale Computerfaciliteiten (National Computing Facilities Foundation, NCF) for the use of supercomputer facilities. Both organizations are financially supported by the Netherlands Organization for Scientific Research (NWO). The support of the Science and Technology Cooperation Germany-Poland, the Polish Committee for Scientific Research (Grant No. 2P03B03914), and the U.S. Department of Energy is gratefully acknowledged. Part of the calculations have been performed on the Cray T90 and T3E of the John von Neumann Institute for Computing, Jülich, Germany.

[1] W. Glöckle, H. Witała, D. Hüber, H. Kamada, and J. Golak, Phys. Rep. **274**, 107 (1996).
[2] J. Carlson and R. Schiavilla, Rev. Mod. Phys. **70**, 743 (1998).
[3] A. Nogga, H. Kamada, and W. Glöckle, Phys. Rev. Lett. **85**, 944 (2000).
[4] W. Glöckle, H. Kamada, J. Golak, H. Witała, S. Ishikawa, and D. Hüber, in *Proceedings of the Second Workshop on Electronuclear Physics with Internal Targets and the BLAST Detector*, edited by R. Alarcon and R. Milner (World Scientific, Singapore, 1999), pp. 185–200, and references therein.
[5] G. Audit *et al.*, Phys. Lett. B **227**, 331 (1989).
[6] G. Audit *et al.*, Phys. Rev. C **44**, R575 (1991).
[7] J.M. Laget, Nucl. Phys. **A446**, 489c (1985).
[8] A.J. Sarty *et al.*, Phys. Rev. C **47**, 459 (1993).
[9] G. Audit *et al.*, Nucl. Phys. **A614**, 461 (1997).
[10] N.R. Kolb *et al.*, Phys. Rev. C **54**, 2175 (1996).
[11] T. Emura *et al.*, Phys. Rev. Lett. **73**, 404 (1994).
[12] T. Emura *et al.*, Phys. Rev. C **49**, R597 (1994).
[13] A. Zondervan *et al.*, Nucl. Phys. **A587**, 697 (1995).
[14] L.J.H.M. Kester *et al.*, Phys. Rev. Lett. **74**, 1712 (1995).
[15] C.J.G. Onderwater *et al.*, Phys. Rev. Lett. **78**, 4893 (1997).
[16] C.J.G. Onderwater *et al.*, Phys. Rev. Lett. **81**, 2213 (1998).
[17] G. Rosner, in *Proceedings of the Conference on Perspectives in Hadronic Physics*, Trieste, 1997 (ICTP/World Scientific, Singapore, 1997), p. 185.
[18] R. Starink *et al.*, Phys. Lett. B **474**, 33 (2000).
[19] D.L. Groep *et al.*, Phys. Rev. Lett. **83**, 5443 (1999).
[20] C. Giusti and F.D. Pacati, Nucl. Phys. **A535**, 573 (1991).
[21] P. Wilhelm, J.A. Niskanen, and H. Arenhövel, Nucl. Phys. **A597**, 613 (1996); Phys. Rev. Lett. **74**, 1034 (1995).
[22] S. Boffi, C. Giusti, F.D. Pacati, and M. Radici, *Electromagnetic Response of Atomic Nuclei* (Clarendon Press, Oxford, 1996).
[23] E. van Meijgaard and J.A. Tjon, Phys. Rev. Lett. **57**, 3011 (1986).
[24] S. Ishikawa, J. Golak, H. Witała, H. Kamada, W. Glöckle, and D. Hüber, Phys. Rev. C **57**, 39 (1998), and references therein.
[25] H. R. Poolman, Ph.D. thesis, Vrije Universiteit, Amsterdam, 1999.
[26] H. Anklin *et al.*, Nucl. Phys. **A636**, 189 (1998).
[27] C.M. Spaltro *et al.*, Phys. Rev. Lett. **81**, 2870 (1998).
[28] J. Golak, H. Kamada, H. Witała, W. Glöckle and S. Ishikawa, Phys. Rev. C **51**, 1638 (1995).
[29] R. Schiavilla, V.R. Pandharipande, and D.O. Riska, Phys. Rev. C **40**, 2294 (1989).
[30] D.O. Riska, Phys. Scr. **31**, 471 (1985).
[31] V.V. Kotlyar, H. Kamada, J. Golak, and W. Glöckle, Few-Body Syst. **28**, 35 (2000).
[32] K. Chmielewski, S. Nemoto, A.C. Fonseca, and P.U. Sauer, Few-Body Syst., Suppl. **10**, 335 (1999).
[33] L. Machenil, M. Vanderhaeghen, J. Ryckebusch, and M. Waroquier, Phys. Lett. B **316**, 17 (1993).
[34] A. Nogga, D. Hueber, H. Kamada, and W. Glöckle, Phys. Lett. B **409**, 19 (1997).

[35] L. de Vries *et al.*, Nucl. Instrum. Methods Phys. Res. A **292**, 629 (1990).
[36] A.R. Pellegrino *et al.*, Nucl. Instrum. Methods Phys. Res. A **437**, 188 (1999).
[37] L.W. Mo and Y.S. Tsai, Rev. Mod. Phys. **41**, 205 (1969).
[38] D. L. Groep, Ph.D. thesis, Universiteit Utrecht, 2000.
[39] Th. Wilbois, P. Wilhelm, and H. Arenhövel, Phys. Rev. C **54**, 3311 (1996).
[40] J. Ryckebusch, L. Machenil, M. Vanderhaeghen, V. van der Sluys, and M. Waroquier, Phys. Rev. C **49**, 2704 (1994).